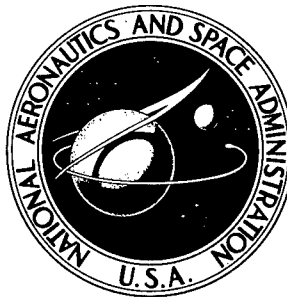


NASA TECHNICAL NOTE



NASA TN D-3468

NASA TN D-3468

Reproduced From  
Best Available Copy

## DIMPLE, SPALL, AND PERFORATION CHARACTERISTICS IN ALUMINUM, COLUMBIUM, AND STEEL PLATES UNDER HYPERVELOCITY IMPACT

*by Nestor Clough  
Lewis Research Center*

*A. R. McMillan  
General Motors Corporation*

*and Seymour Lieblein  
Lewis Research Center*

**DISTRIBUTION STATEMENT A**  
Approved for Public Release  
Distribution Unlimited

20011022 087

NATIONAL AERONAUTICS AND SPACE ADMINISTRATION • WASHINGTON, D. C. • JUNE 1966

22543  
NOV 28 1966

LOVELACE FOUNDATION  
DOCUMENT LIBRARY

DIMPLE, SPALL, AND PERFORATION CHARACTERISTICS IN ALUMINUM,  
COLUMBIUM, AND STEEL PLATES UNDER HYPERVELOCITY IMPACT

By Nestor Clough

Lewis Research Center  
Cleveland, Ohio

A. R. McMillan

General Motors Corporation  
Defense Research Laboratory  
Santa Barbara, Calif.

and Seymour Lieblein

Lewis Research Center  
Cleveland, Ohio

NATIONAL AERONAUTICS AND SPACE ADMINISTRATION

---

For sale by the Clearinghouse for Federal Scientific and Technical Information  
Springfield, Virginia 22151 - Price \$1.00

# DIMPLE, SPALL, AND PERFORATION CHARACTERISTICS IN ALUMINUM, COLUMBIUM, AND STEEL PLATES UNDER HYPERVELOCITY IMPACT

by Nestor Clough, A. R. McMillan\*, and Seymour Lieblein

Lewis Research Center

## SUMMARY

An experimental research program designed to determine the critical damage modes that might be inflicted on various armor materials by the impact of a high-velocity projectile was conducted. The experimental program was performed under NASA contract on a ballistics range facility of the General Motors Corporation, Defense Research Laboratories, Santa Barbara, California. Spherical pyrex projectiles of nominally 2.38- and 3.18-millimeter diameters were accelerated to velocities of approximately 7.6 kilometers per second and impacted against flat-plate targets at room temperature in an evacuated impact chamber. Target thickness at incipient perforation, rear-surface dimple, and spall were determined for plates of AISI 316 stainless steel, 2024-T6 aluminum, and columbium - 1 percent zirconium. The results indicated that the thickness at the onset of each of these damage modes varied significantly with each material. Columbium - 1 percent zirconium showed thicknesses at incipient dimple and spall substantially greater than those for aluminum and stainless steel. The materials coefficient used to correlate crater depth with the modulus of elasticity of the material was also determined. A wide variation in the value of the materials coefficient was found for the three materials impacted.

## INTRODUCTION

The existence of a hazard to space vehicle components from the impact of meteoroids has been recognized as an important factor in the design of such components. An analysis of the meteoroid damage problem for waste-heat radiators of space power systems is

---

\*General Motors Corporation, Defense Research Laboratory.

presented in reference 1, where it is pointed out that the total hazard is a function of two separate factors: first, definition of the meteoroid population in terms of relative impact velocity, rate of meteoroid impact, and meteoroid structure; and second, an understanding of the phenomenon of hypervelocity impact.

In radiator design calculations, the required armor thickness is generally obtained by multiplying the calculated impact crater depth corresponding to the severity of the meteoroid hazard by an arbitrary damage factor (ref. 1). Accurate values of this damage factor as well as a correlation factor involved in the crater depth calculation are not known for specific materials applicable to radiator design. Inasmuch as these factors strongly affect the resultant radiator weight, a better qualitative and quantitative understanding of the hypervelocity-impact process resulting from impact tests on specific armor materials, is necessary.

The general cratering damage likely to be incurred by materials undergoing hypervelocity impact can be obtained, for example, from references 2 to 4; however, little information exists describing the specific damage likely to be incurred by the vulnerable portions of space radiators under operational conditions. Many variables may affect the phenomenon of hypervelocity impact into fluid-carrying space radiators, such as the specific geometry, the materials used for the tubes and armor protection, the operating temperature, and the presence of a liquid or gas in the tube.

Initial results of impacts into space radiator target configurations of various materials are reported in reference 5. It was significantly established in reference 5 that there are damage modes other than complete perforation of the radiator tube that may be critical to the successful operation of the radiator. In particular, it was shown in reference 5 that the inner surface of a tube could be made to dimple and spall with armor thicknesses significantly greater than the crater depth. Hence, simple cratering is not the only critical design condition for fluid-carrying tubes, and the effects of other variables on inner-surface dimple, spall, and perforation need to be studied. The results of an investigation of the effect of the type of armor material on the total damage in flat-plate targets are presented.

Reported herein are the results of an experimental hypervelocity-impact program in which flat-plate targets of three materials were impacted at room temperature with two different projectile sizes at a nominally constant velocity. The plate thickness was varied to determine the degree of total damage. The targets tested consisted of flat plates of 2024-T6 aluminum, AISI 316 stainless steel, and columbium - 1 percent zirconium. These targets were impacted with pyrex spheres of 0.016 or 0.040 gram mass at a nominal velocity of 7.6 kilometers per second. The target thickness was varied so that the threshold limits of perforation, spall, and dimple could be defined. The experimental program was conducted by the General Motors Corporation, Defense Research Laboratories, Santa Barbara, California under NASA contract numbers NASw-468 and NAS3-2798.

## RESULTS AND DISCUSSION

All tests were conducted on a ballistic range, which is fully described in reference 6. The basic equipment consists of a 30-caliber accelerated-reservoir light-gas gun, a 6-meter free-flight range, and an impact chamber. The materials tested were 316 stainless steel, 2024-T6 aluminum, and columbium - 1 percent zirconium and were obtained as bars nominally 10 centimeters square. The targets were cut from these bars in varying thicknesses as required. The experimental procedure involved impacting flat-plate targets having progressively less thickness until complete perforation of the target was visible to the unaided eye. The targets were then sectioned at the point of maximum crater depth and examined. Generally, each target material required five to eight impacts each at a different thickness to define the regimes of dimple, spall, and perforation. The targets were impacted at room temperature with either a 2.38- or 3.18-millimeter-diameter pyrex projectile with masses of nominally 0.016 or 0.040 gram, respectively, at a velocity in the range from 7.0 to 7.9 kilometers per second (kinetic energies from  $3.92 \times 10^9$  to  $1.25 \times 10^{10}$  ergs).

### Target Damage

In addition to measurements of the penetration, or crater depth,  $P$  the total target damage was noted. Definitions of the damage modes of interest, as they are used herein, are shown in figure 1. Dimple is defined as any measurable displaced movement of the free surface below the crater without dislodgment of material, which in a radiator tube, will result in a restriction of the flow. Spall is defined as the condition that results in a breaking away of fragments of the rear surface of the target below the crater. In a fluid circuit in zero-g operation such metal particles can cause serious damage to rotating components. Perforation is used in the conventional sense of a visible puncture through which working fluid can leak out and escape. In these tests, the objective was to define the points of incipient rear-surface damage; hence, the degree of dimple, spall, or perforation was estimated and reported. Visual observations of the sectioned targets were used to classify the degree of damage.

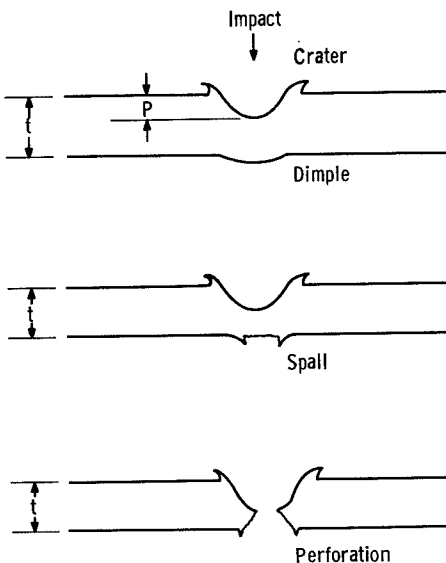


Figure 1. - Definition of significant damage modes in flat plates.

A complete tabulation of all the shots fired in

TABLE I. - ORIGINAL DATA FOR IMPACT STUDY

Target material	Target thickness, t, cm	Projectile mass, m, g	Projectile velocity, V, km/sec	Measured penetration depth, P, cm	Rear-surface damage	Reference semi-infinite penetration depth, $P_{\infty}^*$ , cm	Corrected semi-infinite penetration depth, $P_{\infty}$ , cm	Ratio of target thickness to semi-infinite penetration depth, $t/P_{\infty}$	Impact round number
AISI 316 Stainless steel	0.454	0.0163	7.60	-----	Perforation	0.328	0.330	1.38	D-519
	.508	.0156	7.69	0.366	Spall	↓	.328	1.55	D-486
	.569	.0159	7.60	.325	Spall		.328	1.74	D-480
	.610	.0163	7.71	.330	Spall		.330	1.85	D-483
	.762	.0156	7.69	.325	Dimple		.328	2.32	D-487
2024-T6 Aluminum	0.825	0.0160	7.56	-----	Perforation	0.519	0.516	1.65	D-488
	.839	.0157	7.30	-----	Perforation	↓	.500	1.68	D-489
	.953	.0163	7.45	0.555	Spall		.510	1.85	D-514
	1.142	.0157	7.65	.523	Spall		.516	2.22	D-482
	1.194	.0156	7.56	.515	Dimple		.509	2.35	D-481
	1.208	.0178	7.50	.483	Dimple		.528	2.28	D-963
	1.227	.0157	7.32	.498	Dimple		.500	2.45	D-478
Columbium - 1 percent zirconium	0.701	0.0421	7.16	-----	Perforation	0.430	0.414	1.69	D-1129
	.762	.0415	7.62	0.580	Spall	↓	.432	1.77	D-1077
	.889	.0415	7.56	.424	Spall		.429	2.07	D-1076
	1.017	.0420	6.95	.406	Spall		.406	2.50	D-1130
	1.152	.0418	7.10	.434	Spall		.414	2.78	D-1131
	1.398	.0418	7.14	.416	Spall		.414	3.38	D-1194
	1.650	.0405	7.32	.404	Spall		.416	3.96	D-1195
	1.905	.0412	7.50	.381	Dimple		.426	4.47	D-1196
	1.146	.0162	7.50	.290	Slight spall		.310	3.73	D-1496
	1.248	.0163	7.41	.288	Slight dimple		.310	4.09	D-1495
	.462	.0160	7.00	-----	Perforation		.310	1.58	D-1549

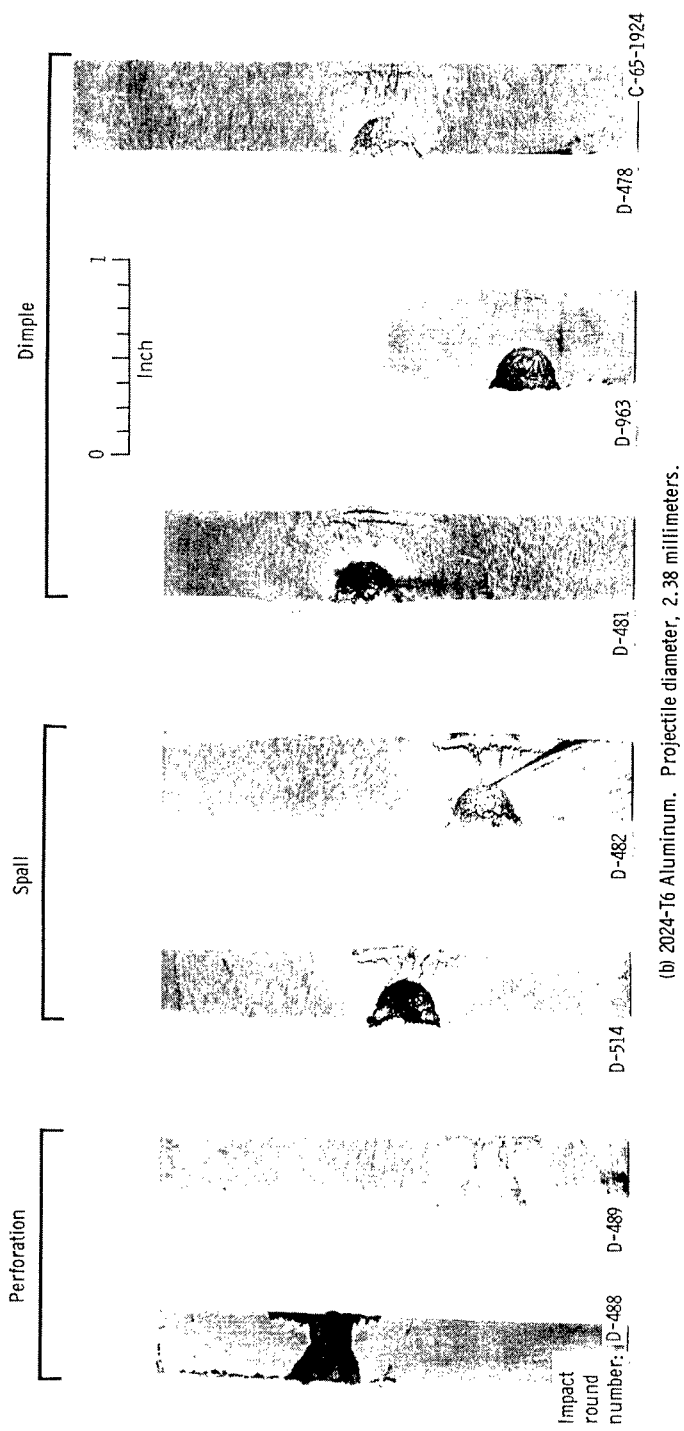
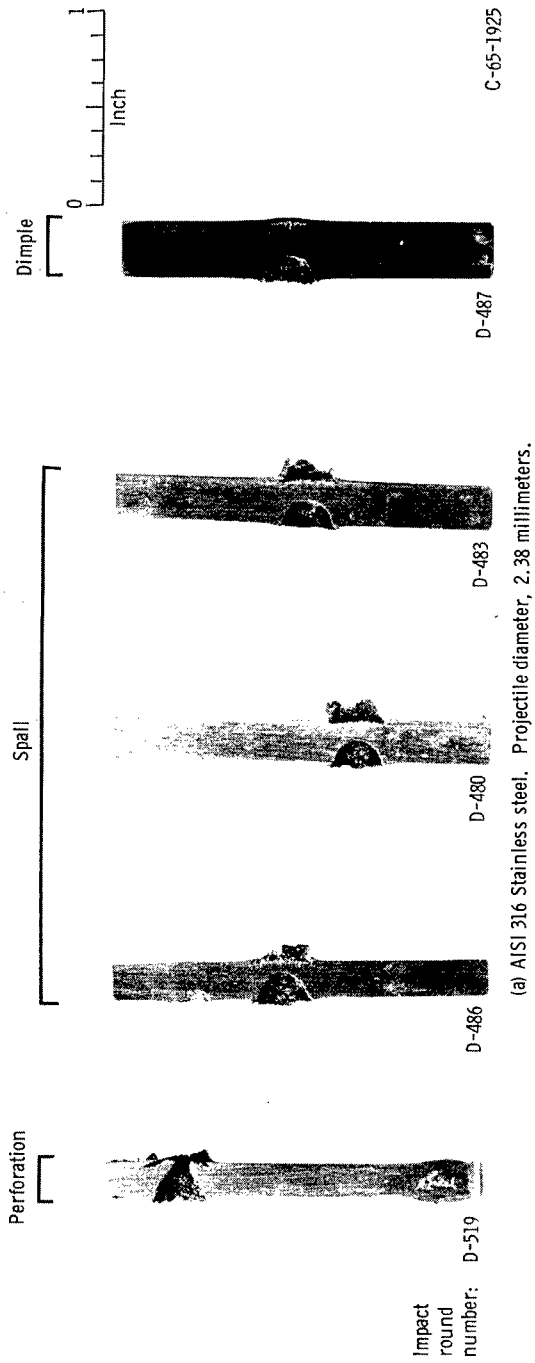
conjunction with this investigation is given in table I. The table includes a description of the targets impacted (i. e. , material and plate thickness), impacting projectile mass and velocity, measured penetration depth, a qualitative description of the degree of rear-surface damage sustained by the targets, and values to be used in determining damage thickness factors. Targets sectioned after impact are shown for each material in figure 2. The figures clearly depict the transition from simple penetration (cratering) to perforation, with varying degrees of spall between these limits.

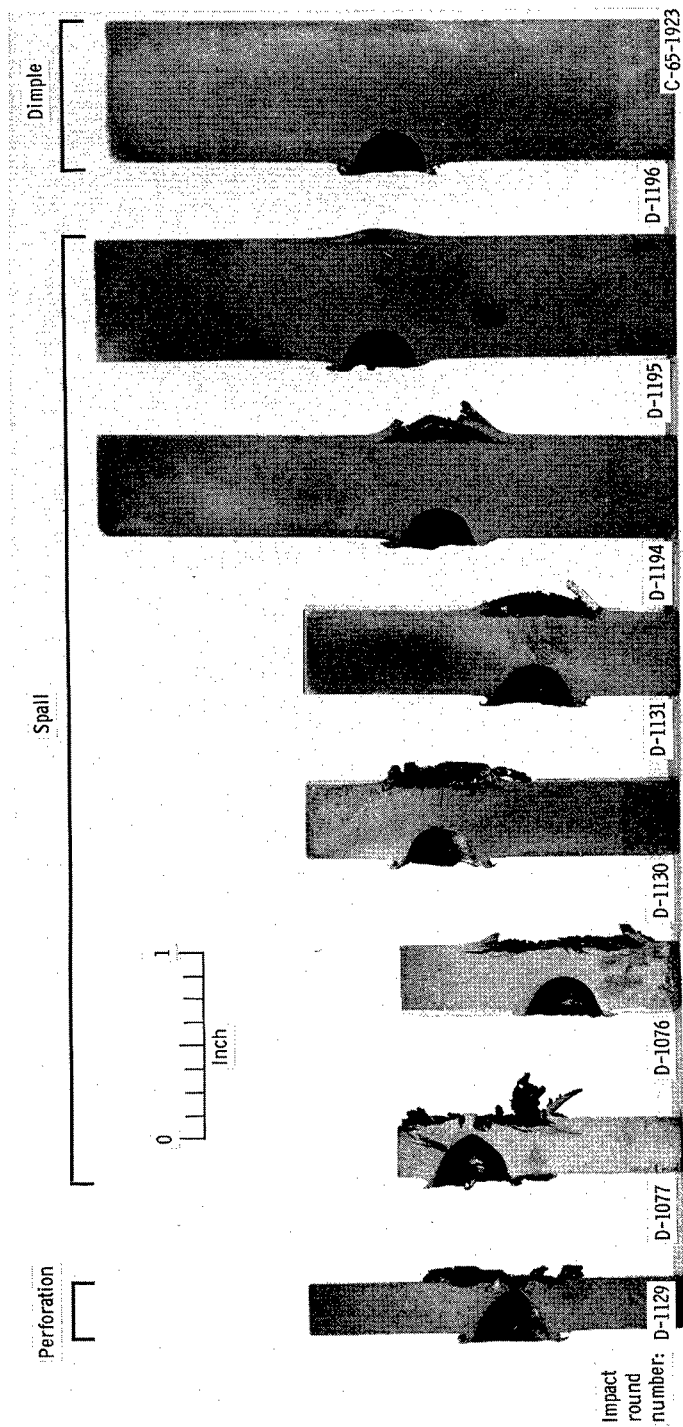
Examination of figure 2 shows qualitatively the effect of different materials on the nature of the target damage. The aluminum in figure 2(b) shows a brittle type of fracture evidenced by the absence of any lips extended above the target surface around the spall region or the crater. The stainless steel (fig. 2(a)) and columbium alloy (figs. 2(c) and (d)) both show ductile type fracture evidenced by the crater lips and fairly smooth spall fracture and spall lips.

According to reference 7, the spall characteristic is associated with the stress-wave phenomena in the target. When a projectile strikes a solid target at high speed, a shock wave is generated that becomes approximately spherical in shape after a short period of time. The shock decays in strength as it propagates through the target and ultimately becomes a compressive elastic wave. When the stress wave encounters the rear surface, it is reflected as a tensile stress wave whose magnitude may be sufficient to cause the rear surface of the target to spall or dimple.

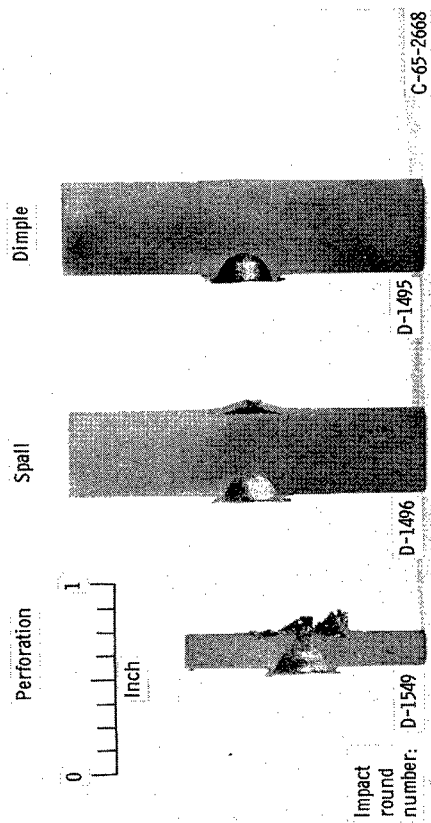
As the target thickness is reduced or as the impact velocity is increased, the thickness of the spall is increased and ultimately meets the crater resulting in a puncture. At the other extreme, where the target is sufficiently thick in relation to the severity of the impact, the stress wave will decay to a low enough stress level so that the material can sustain the reflected tensile stress with no observable rear-surface damage. In between these two extremes lie the regions of spall and dimple, where the target thickness is such that the magnitude of the reflected tensile wave will exceed the strength of the material and a local deformation and fracture will occur. Dependent on material properties, this fractured section of the target will either separate as a spall or remain as a dimple.

Various attempts have been made to analyze the spall problem (e. g. , refs. 7 to 10); however, no generalized solution to the problem has been successfully obtained since the problem of defining thickness at which spall will occur depends on several undefined material properties. The problem treated to date has been in general the definition of the local point of incipient spall (i. e. , the first occurrence of an internal crack). The definition of when and how particles will detach from the rear surface of the target has not, as yet, been treated analytically.





(c) Columbium - 1 percent zirconium. Projectile diameter, 3.18 millimeters.



(d) Columbium - 1 percent zirconium. Projectile diameter, 2.38 millimeters.

Figure 2. - Dimple, spall, and perforation in flat-plate targets impacted with pyrex spheres. Projectile impact velocity, 7.6 kilometers per second. Targets were sectioned after impact.

TABLE II. - CALCULATION OF REFERENCE SEMI-INFINITE PENETRATION DEPTH

Target material	Projec- tile mass, m, g	Projec- tile velocity, V, km/sec	$\left(\frac{m}{m^*}\right)^{1/3}$	$\left(\frac{V}{V^*}\right)^{2/3}$	Mea- sured semi- infinite pene- tration depth, $P_{\infty}$ , cm	Refer- ence semi- infinite pene- tration depth, $P_{\infty}^*$ , cm	Impact round number
Columbium - 1 percent zirconium	0.0418	7.10	1.000	0.953	0.434	0.456	D-1131
	.0418	7.14	1.000	.957	.416	.436	D-1194
	.0405	7.32	.990	.973	.404	.421	D-1195
	.0412	7.50	.995	.989	.381	.390	D-1196
Average						0.430	
AISI 316 Stainless steel	0.0163	7.71	1.007	1.008	0.330	0.327	D-483
	.0156	7.69	.991	1.005	.325	.329	D-487
Average						0.328	
2024-T6 Aluminum	0.0156	7.56	0.991	0.995	0.515	0.523	D-481
	.0157	7.32	.994	.974	.498	.516	D-478
Average						0.519	

### Damage Thickness Factors

From examination of the sectioned targets of figure 2, it was possible to estimate the thickness corresponding to the onset of perforation, spall, and dimple for the particular energy level of the series of impacts, and to express each thickness as a dimensionless parameter. The parameter is termed the damage thickness factor and is defined as the ratio of target thickness at incipient dimple, spall, or perforation to the penetration depth in a semi-infinite target  $P_{\infty}$ .

The measured values of the penetration depth  $P$  could not in all cases be considered equal to  $P_{\infty}$  since many of the targets were essentially thin plates that either spalled severely or perforated. In order to arrive at values of  $P_{\infty}$  for the various targets impacted, a reference value of  $P_{\infty}^*$  was employed for each target material. The quantity  $P_{\infty}^*$  is the value of the penetration depth in a semi-infinite target at the following reference impact conditions: projectile velocity  $V^*$ , 7.62 kilometers per second; projectile mass  $m^*$ , 0.0160 gram for the 2.38-millimeter-diameter projectile and 0.0418 gram

for the 3.18-millimeter-diameter projectile. An average value of  $P_{\infty}^*$  was obtained, as shown in table II, for each material. Since values of projectile mass and velocity for each impact varied somewhat from the above reference values (see table I), corresponding values of  $P_{\infty}$  were obtained from  $P_{\infty}^*$  with a correction based on the assumption that crater volume varies with projectile kinetic energy (refs. 4 and 5).

The relation between crater volume and projectile kinetic energy based on the assumption of hemispherical craters can be expressed in an equation of the form (ref. 5)

$$P_{\infty} = \gamma \left( \frac{\rho_p}{\rho_t} \right)^{\varphi} \left( \frac{V}{C} \right)^{2/3} d \quad (1)$$

(All symbols are defined in the appendix.) For equal-density projectiles impacting targets made from the same material, the relation becomes

$$P_{\infty} = P_{\infty}^* \left( \frac{V}{V^*} \right)^{2/3} \left( \frac{m}{m^*} \right)^{1/3} \quad (2)$$

In this experiment,  $P_{\infty}^*$ ,  $V^*$ , and  $m^*$  are the reference values specified in the preceding paragraph. The calculated values of  $P_{\infty}$  were then used in determining the ratio  $t/P_{\infty}$  for each impact, as shown in table I.

The parameter  $P/P_{\infty}$  is shown plotted against  $t/P_{\infty}$  in figure 3 for each material tested. The regions of perforation, spall, and dimple appear on the figures, and the transition point from one region to another was estimated by visual observation and comparison of the sectioned targets after impact. When the path of the curves is traced from the origins, the straight  $45^\circ$  portion is termed the penetration line, since along the line, the penetration depth is equal to the target thickness. The value of  $t/P_{\infty}$  for incipient perforation is established from the curves at the maximum value of  $P/P_{\infty}$ . Beyond the maximum value of  $P/P_{\infty}$  the curves drop abruptly to  $P/P_{\infty} = 1.0$ . For all three materials, the curves indicate that shortly after spall begins, the penetration depth becomes unaffected by the presence of spall or dimple and remains equal to the semi-infinite penetration depth (cratering line). The estimated points of incipient spall and dimple also appear on the curves.

The curve for stainless steel (fig. 3(a)) shows complete perforation of the target up to a target thickness of  $1.4 P_{\infty}$ . From a thickness of  $1.4 P_{\infty}$  to about  $1.9 P_{\infty}$  the target spalled from the rear surface. From  $1.9 P_{\infty}$  to about  $2.35 P_{\infty}$  the target dimpled. The aluminum showed the same general trends as the steel but with different ratio values (fig. 3(b)). Perforation of the target occurred up to a thickness of about  $1.7 P_{\infty}$ . From about  $1.7 P_{\infty}$  to about  $2.3 P_{\infty}$  the target spalled. For this material the dimple range was found to be from  $2.3 P_{\infty}$  to  $2.5 P_{\infty}$ , which is small in comparison with steel. The

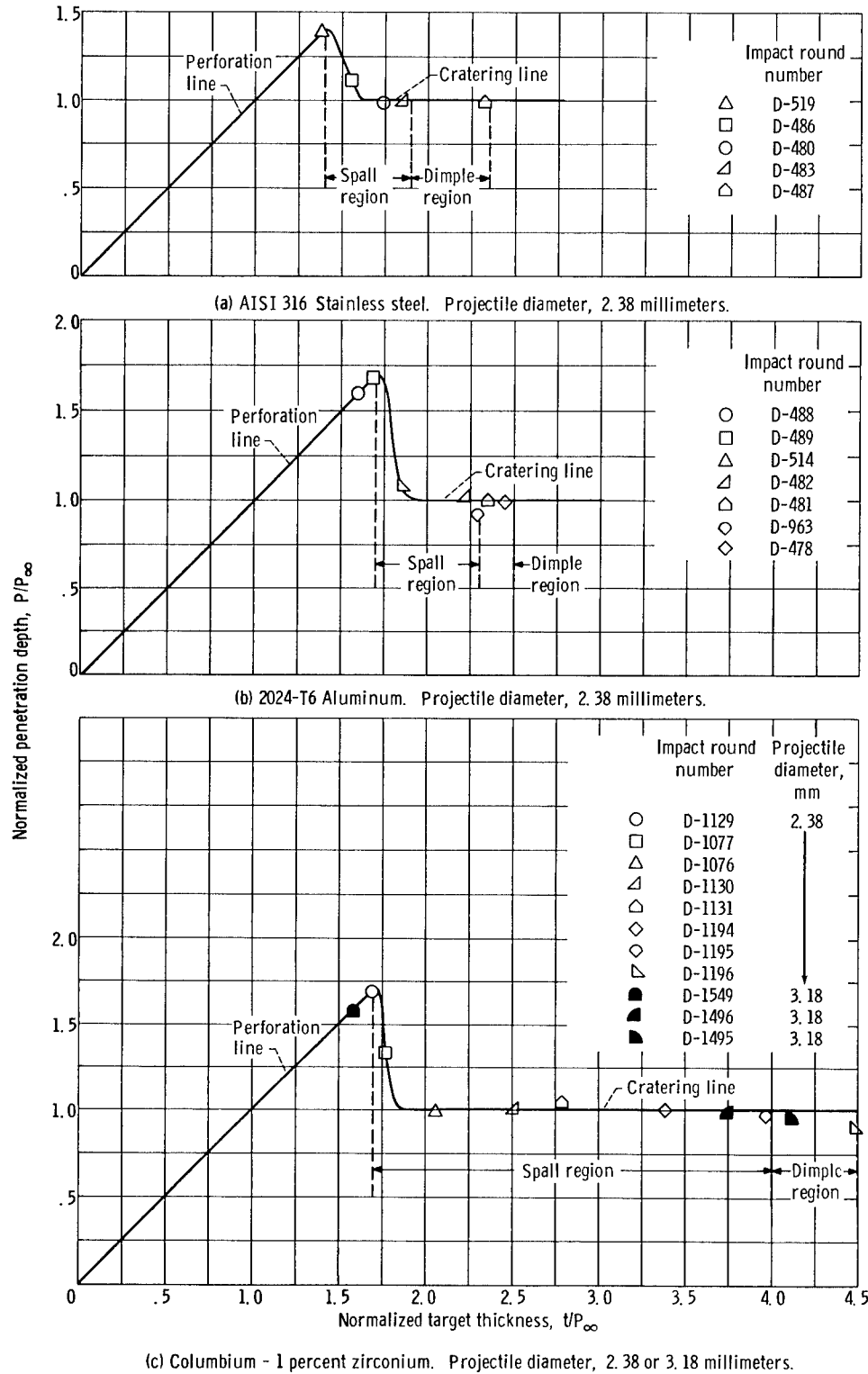


Figure 3. - Damage region curves for flat-plate targets impacted at room temperature with pyrex spheres. Projectile impact velocity, 7.6 kilometers per second.

columbium alloy (fig. 3(c)) for both projectile sizes follows the same general trend as that of aluminum; however, a much larger spall region was found than that found for both the stainless steel and the aluminum tested. The columbium perforated up to about  $1.7 P_{\infty}$  and then spalled from  $1.7 P_{\infty}$  to about  $4.0 P_{\infty}$ . As in the aluminum targets, a small dimple regime was found with dimpling occurring from about  $4.0 P_{\infty}$  to  $4.5 P_{\infty}$ . The close agreement between the damage thickness factors for the two different projectile sizes for the columbium alloy targets also indicates that, within the limits of projectile masses used herein, the damage thickness factors can be scaled and the incipient damage thickness determined if  $P_{\infty}$  is known.

Comparison of the results of the impacts into steel, aluminum, and columbium indicate that all three modes of damage vary considerably for the materials tested. The thicknesses at perforation, spall, or dimpling are not in the same ratios for the three materials tested, which indicates that different material properties are dominant in the three different types of damage modes. For example, the ratios of threshold perforation thickness to threshold spall thickness for the steel, aluminum, and columbium tested are 0.75, 0.7, and 0.44, respectively. The ratios of threshold perforation thickness to threshold dimple thickness are 0.62, 0.70, 0.38 for steel, aluminum, and columbium, respectively. Furthermore, the results of figure 3 show that the thickness ratio  $t/P_{\infty}$  at perforation is not a constant value. (A value of thickness of  $1.5 P_{\infty}$  to prevent perforation has been widely used and quoted in the literature, e. g., ref. 11.) Apparently, this value, too, is a function of the target material.

Realistic comparisons of the ability of these three materials to prevent critical damage are best made on the basis of mass per unit of exposed area. The various thicknesses for each of the materials tested at incipient dimple, spall, and perforation for the reference impact conditions (e. g., impact velocity of 7.62 km/sec and projectile mass of 0.016 g) were multiplied by the respective material densities. The results are shown in table III. On this basis of comparison, 2024-T6 aluminum can protect a given area with the least mass while columbium - 1 percent zirconium alloy requires the greatest mass.

TABLE III. - TARGET MASS PER UNIT AREA  
AT INCIPIENT DAMAGE

Material	Mass per unit area at incipient damage, $t^* \rho_t$ , g/cm <sup>2</sup>		
	Dimple	Spall	Perforation
2024-T6 Aluminum	3.51	3.22	2.38
AISI 316 Stainless steel	6.17	4.98	3.67
Columbium - 1 percent zirconium	11.30	10.10	4.24

It should be noted that the damage factors defined in the preceding discussion refer to incipient or threshold damage conditions and are not directly suitable as design values to prevent a given damage mode. An increase in the magnitude of each factor is necessary to provide a margin of safety to insure that the damage mode in question be avoided. For example, a design that would prevent perforation may incorporate an armor thickness that was sized by the spall damage factor. Similarly, the dimple damage factor might be used as a criterion for the prevention of spall. The extent that a particular critical damage factor is augmented is largely a matter of individual judgement.

### Materials Coefficient for Penetration Depth

The estimation of the depth of penetration in a thick (semi-infinite) target due to spherical impacting particles has been made with various empirical equations. One such equation based on the modulus of elasticity reported in reference 5 is given by equation (1). The use of a relation of the form of equation (1) involves an experimental materials coefficient  $\gamma$  that has been reported to vary from about 1.5 to 2.5 (refs. 1 and 5). In reference 1, an average value of  $\gamma = 2.0$  for an exponent  $\phi = 1/2$  was proposed for use in the absence of an explicit value for the specific target material. A value of  $\gamma = 2.28$  was proposed in reference 11 as obtained from lead and copper targets for  $\phi = 2/3$ .

The data obtained in the thicker flat plates of this program were utilized to calculate the materials coefficient for the preceding materials since the crater depth in these cases closely represents  $P_{\infty}$  (fig. 3). The materials coefficient (eq. (1)) can be written as

$$\gamma = \frac{\frac{P}{d}}{\left(\frac{\rho_P}{\rho_t}\right)^{\phi} \left(\frac{V}{C}\right)^{2/3}} \quad (3)$$

where  $P/d$  is the ratio of measured depth of penetration to projectile diameter. The other values in the denominator are computed from the material properties and test conditions (ref. 1 recommends  $\phi = 1/2$ ; while ref. 12 uses  $\phi = 2/3$ ). The target material sonic velocity  $C$  in equation (3) was calculated as  $\sqrt{E/\rho_t}$ . The values of Young's modulus  $E$  used in the computation are given in table IV.

Values of  $\gamma$  were computed for the applicable data points as indicated in table IV for the 316 stainless steel, 2024-T6 aluminum, and columbium - 1 percent zirconium targets.

TABLE IV. - CALCULATION OF MATERIALS COEFFICIENT

Target material	Target density, $\rho_t'$ g/cm <sup>3</sup>	Projec- tile velocity, V, km/sec	Projec- tile density, $\rho_p'$ g/cm <sup>3</sup>	Projec- tile diameter, d, mm	Measured penetra- tion depth, P, cm	Ratio of penetration depth to projectile diameter, P/d	Target modulus of elasticity, E, dyne/cm <sup>2</sup>	Target sonic velocity, C, km/sec	$\left(\frac{\rho_p}{\rho_t}\right)^{1/2}$	$\left(\frac{\rho_p}{\rho_t}\right)^{2/3}$	$\left(\frac{V}{C}\right)^{2/3}$	Material coefficient, $\gamma$		Impact round number
												Exponent $\varphi$		
												1/2	2/3	
AISI 316 Stainless steel	8.0	7.6 7.71 7.69 7.69	2.27	2.38	0.325 .33 .366 .325	1.365 1.39 1.54 1.36	a <sub>19.5</sub> ×10 <sup>11</sup>	4.91	0.532	0.431	1.31 1.35 1.348 1.348	1.92 1.94 2.14 1.90	2.42 2.39 2.65 2.35	D-488 D-483 D-486 D-487
Average														
2024-T6 Aluminum	2.7	7.32 7.56 7.65 7.45 7.5	2.27	2.38	0.498 .515 .523 .555 .483	2.09 2.16 2.20 2.33 2.02	a <sub>7.04</sub> ×10 <sup>11</sup>	5.10	0.916	0.891	1.27 1.30 1.31 1.29 1.29	1.80 1.81 1.83 1.97 1.71	1.85 1.86 1.88 2.02 1.76	D-478 D-481 D-482 D-514 D-963
Average														
Columbium - 1 percent zirconium	8.05	7.1 6.95 7.56 7.14 7.32 7.50 7.50 7.41	2.47	3.18	0.434 .406 .424 .416 .404 .381 .290 .288	1.37 1.28 1.34 1.31 1.27 1.20 1.22 1.21	b <sub>11.0</sub> ×10 <sup>11</sup>	3.71	0.554	0.454	1.545 1.525 1.61 1.55 1.575 1.60 1.60 1.59	1.63 1.52 1.50 1.52 1.45 1.35 1.43 1.43	1.99 1.85 1.83 1.86 1.78 1.65 1.77 1.77	D-1131 D-1130 D-1076 D-1194 D-1195 D-1196 D-1496 D-1495
Average														
1.47 1.81														

<sup>a</sup>From ref. 14.<sup>b</sup>From ref. 15.

Values of  $\gamma$  corresponding to  $\phi = 1/2$  and  $2/3$  were calculated. For the four steel targets, average values of  $\gamma$  of 1.98 for  $\phi = 1/2$  and of 2.45 for  $\phi = 2/3$  were obtained. For the 2024-T6 aluminum targets, average values of  $\gamma$  of 1.83 and 1.86 for  $\phi = 1/2$  and  $2/3$ , respectively, were obtained. These values of the materials coefficient obtained for the 2024-T6 aluminum are substantially less than the value of  $\gamma = 2.27$  ( $\phi = 1/2$  and  $2/3$ ) obtained for 356-T51 cast aluminum in reference 5. The values of the materials coefficient for the columbium - 1 percent zirconium are 1.47 and 1.81 for  $\phi = 1/2$  and  $2/3$ , respectively. These values correspond to the previously reported values of  $\gamma = 1.49$  and 1.79 determined for the same target material in reference 5.

The wide differences in  $\gamma$  among the three materials tested and for the cast and wrought aluminum (which have essentially equal densities and moduli) indicate that a material strength parameter or parameters other than the modulus of elasticity may be of significance in determining the penetration of a projectile at high velocities. However, the establishment of the parameters are beyond the scope of this investigation.

### Perforation Thickness Correlation

In reference 13, target thickness at incipient perforation was correlated with the density and percent elongation of the target material. The targets tested included a wide range of material densities and ductilities and were impacted at room temperature over a range of velocities from less than 2 to more than 6 kilometers per second with 1.59-millimeter-diameter 2017-T4 aluminum projectiles.

From the data of reference 13, the following representation of threshold perforation thickness can be made:

$$\frac{t^*}{d} = K \left( \frac{1}{\epsilon} \right)^{1/18} \left( \frac{1}{\rho_t} \right)^{1/2} V \quad (4)$$

where  $t^*$  is the thickness at threshold perforation,  $d$  is the projectile diameter,  $K$  is a correlating constant,  $\epsilon$  is the percent elongation of a 2-inch specimen,  $\rho_t$  is the target density, and  $V$  is the projectile velocity. It should be noted, however, that equation (4) was obtained from tests with a single projectile size and material.

The perforation thicknesses obtained in the tests conducted herein can be compared with the results of reference 13. The ratio of thickness at perforation to projectile diameter is plotted in figure 4 against the correlating parameter of equation (4) for the columbium alloy, steel, and aluminum tested herein with pyrex projectiles. Values of percent elongation used were 7, 12, and 40 percent for the aluminum, columbium - 1 percent zirconium, and stainless steel, respectively. A straight line (dashed line in fig. 4)

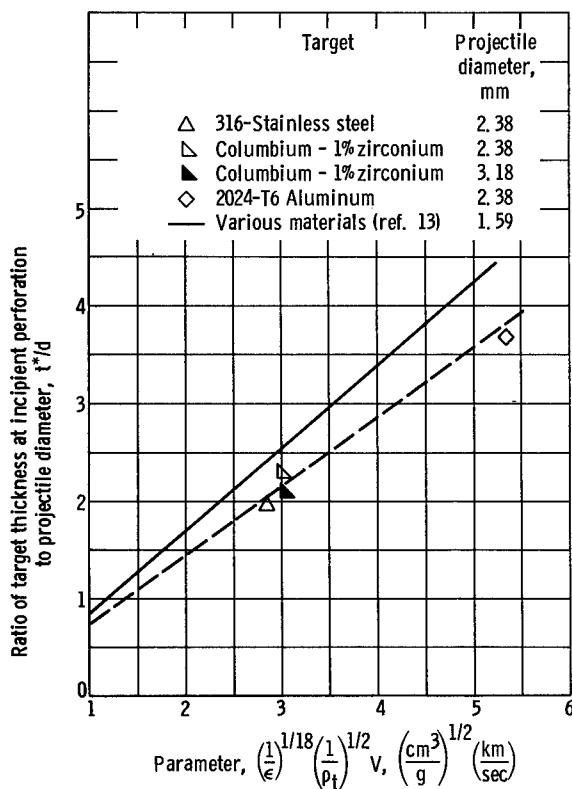


Figure 4. - Correlation of target thickness at threshold perforation for 316 stainless steel, 2024-T6 aluminum, and columbium - 1 percent zirconium.

can be drawn through the origin and the test points that falls below the curve representing the data of reference 13. This can be expected for two reasons. First the definition of threshold perforation used in reference 13 differed from the definition used herein. In reference 13 threshold perforation was defined as the point at which a given specimen was sufficiently damaged so that it would no longer sustain a pressure differential of a few atmospheres without leaking. This often occurred without a visible hole through the target. The definition used herein requires a complete visible perforation through the target. The second possible reason for the difference in the two curves may be the different projectile materials and sizes used in the experiments, since the correlating variables of equation (4) do not include variations in projectile properties. An indication of the effect of projectile size for like projectile materials can be obtained from the colum-

bium threshold perforation points. The values of  $t^*/d$  for both the 3.18- and 2.38-millimeter-diameter projectiles are in fairly close agreement, as shown in figure 4.

The experiments reported herein cannot specifically confirm the linear velocity variation of equation (4) since all impacts were at nominally the same velocity (7.6 km/sec). However, if this linear relation with velocity is valid, the damage thickness factors for perforation reported in the previous section as a function of  $P_\infty$  may be unique for the particular velocity of impact used in these tests, since  $P_\infty$  was taken to vary with the velocity of impact raised to the 2/3 power (eq. (1)). Thus, a linear relation of perforation thickness with velocity indicates that the damage thickness factor  $t^*/P_\infty$  for perforation might tend to increase with increasing velocity.

Another implication of the preceding results is the apparent successful ability to predict perforation thickness from static material properties with a single empirical correlation parameter. A comparable result could not be obtained for the case of dimple and spall. For the three materials tested and reported herein, no unique correlation for spall thickness could be made on the basis of the variables proposed by reference 13 for threshold perforation.

## SUMMARY OF RESULTS

The various damage thickness factors and materials coefficients were determined for the 2024-T6 aluminum, columbium - 1 percent zirconium, and 316 stainless steel target plates impacted at room temperature and are summarized in the following table:

Material	Rear surface damage factors, $t^*/P_\infty$			Crater depth	
	Dimple	Spall	Perforation	Materials coefficient, $\gamma$	
				Exponent $\phi$	
				1/2	2/3
2024-T6 Aluminum	2.50	2.3	1.7	1.83	1.86
AISI 316 Stainless steel	2.35	1.9	1.4	1.98	2.45
Columbium - 1 percent zirconium	4.50	4.0	1.7	1.47	1.81

The damage thickness factors for incipient dimple, spall, and perforation, and the materials coefficient for depth of penetration varied significantly for the three materials tested. Different material properties are dominant for each damage mode. A strength parameter other than the modulus of elasticity may be of significance in determining the depth of penetration of a projectile at high velocities.

Threshold perforation thicknesses determined for columbium - 1 percent zirconium alloy with two different projectile sizes agree closely. Also, it appears that for impacts at room temperature, target thickness at threshold perforation can be correlated with the percent elongation and density of the target material; however, spall thickness and crater depth do not correlate on the basis of the same relation.

Lewis Research Center,  
National Aeronautics and Space Administration,  
Cleveland, Ohio, March 29, 1966.

## APPENDIX - SYMBOLS

C	target material sonic velocity, $\sqrt{\frac{E}{\rho_t}}$ , km/sec <i>7 cm/sec</i>	t	target thickness, cm
d	projectile diameter, mm or cm	t*	target thickness at incipient rear-surface damage, cm
E	Young's modulus of elasticity for target, dynes/cm <sup>2</sup>	V	projectile velocity, km/sec
K	constant	$\rho_p$	projectile density, g/cm <sup>3</sup>
m	projectile mass, g	$\rho_t$	target density, g/cm <sup>3</sup>
m*	reference projectile mass, g	$\phi$	exponent in cratering equation, 1/2 or 2/3
P	measured penetration depth in target, cm	$\epsilon$	elongation of 2-in. specimen, percent
P <sub>∞</sub>	corrected penetration depth in thick (semi-infinite) target, $P_{\infty}^* \left( \frac{m}{m^*} \right)^{1/3} \left( \frac{V}{V^*} \right)^{2/3}$ , cm	$\gamma$	materials coefficient
P <sub>∞</sub> *	reference penetration depth in semi-infinite target (m = 0.0160 or 0.0418 g and V = 7.62 km/sec), cm		

$$\sqrt{\frac{\text{dynes cm}^2}{\text{cm}^2 \text{ g}}}$$

$$\frac{\text{g cm cm}}{\text{sec}^2 \text{ g}} \quad \text{cm/sec}$$

## REFERENCES

1. Loeffler, I. J.; Lieblein, Seymour; and Clough, Nestor: Meteoroid Protection for Space Radiators. Power Systems for Space Flight. Progress in Astronautics and Aeronautics, Vol. 11, M. Zipkin and R. N. Edwards, eds., Academic Press, Inc., 1963, pp. 551-579.
2. Bjork, R. L.: Meteoroids vs. Space Vehicles. ARS J., vol. 31, no. 6, June 1961, pp. 803-807.
3. Jaffe, Leonard D.; and Rittenhouse, John B.: Behavior of Materials in Space Environments. ARS J., vol. 32, no. 3, Mar. 1962, pp. 320-346.
4. Eichelberger, R. J.; and Gehring, J. W.: Effects of Meteoroid Impacts in Space Vehicles. ARS J., vol. 32, no. 10, Oct. 1962, pp. 1583-1591.
5. Lieblein, Seymour; Clough, Nestor; and McMillan, A. R.: Hypervelocity Impact Damage Characteristics in Armored Space Radiator Tubes. NASA TN D-2472, 1964.
6. Anon.: Aerospace Research Capabilities. Rept. No. TR 63-223 rev., Defense Res. Labs., General Motors Corp., April 1964.
7. Rae, William J.: Comments on the Solution of the Spall-Fracture Problem in the Approximation of Linear Elasticity. Rept. No. CAL-A1-1821-A3, Cornell Aero. Lab. (NASA CR-54250), Jan. 1965.
8. Rinehart, John S.: Practical Countermeasures for the Prevention of Spallation. Rept. No. TR 60-7, Air Force Special Weapons Center, Feb. 1960.
9. Charest, J. A.: Measurements of Shock Wave Pressures Generated by Hypervelocity Impacts in Aluminum. Defense Res. Labs. Rept. No. TR64-58, General Motors Corp., Nov. 1964.
10. Kinslow, Ray: Properties of Spherical Stress Waves Produced by Hypervelocity Impact. Rept. No. AEDC-TDR-63-197, Aro, Inc., Oct. 1963.
11. Bjork, R. L.: Effects of Meteoroid Impact on Steel and Aluminum in Space. Rept. No. P-1662, Rand Corp., Dec. 16, 1958.
12. Summers, James L.; and Charters, A. C.: High-Speed Impact of Metal Projectiles in Targets of Various Materials. Paper Presented at Proc. of Third Hypervelocity Impact Symposium, Armour Res. Foundation, Chicago (Ill.), Oct. 7-9, 1958.
13. Fish, Richard H.; and Summers, James L.: The Effect of Material Properties on Threshold Penetration. Paper presented at Seventh Hypervelocity Impact Symposium, Tampa, Fla., Nov. 1964. (Available as NASA TM X-54786, 1964.)

14. Weiss, V.; and Sessler, J. G., eds.: Aerospace Structural Metals Handbook.  
Vol. I - Ferrous Alloys. Vol. II - Nonferrous Alloys. Second rev. ed., Syracuse Univ. Press, Mar. 1965.
15. Schmidt, F. F.; and Ogden, H. R.: The Engineering Properties of Columbium and Columbium Alloys. Rept. No. DMIC-188, Battelle Memorial Inst., Sept. 6, 1963.